Stochastic Turing patterns on a network

Malbor Asslani
Dipartimento di Scienza e Alta Tecnologia, Università degli Studi dell'Insubria, via Valleggio 11, 22100 Como, Italy

Francesca Di Patti and Duccio Fanelli
Dipartimento di Energetica "Sergio Stecco," Università degli Studi di Firenze, via S. Marta 3, 50139 Firenze, Italy and Istituto Nazionale di Fisica Nucleare, Sezione di Firenze, via G. Sansone 1, 50019 Firenze, Italy

(Received 6 April 2012; published 12 October 2012)

The process of stochastic Turing instability on a scale-free network is discussed for a specific case study: the stochastic Brusselator model. The system is shown to spontaneously differentiate into activator-rich and activator-poor nodes outside the region of parameters classically deputed to the deterministic Turing instability. This phenomenon, as revealed by direct stochastic simulations, is explained analytically and eventually traced back to the finite-size corrections stemming from the inherent graininess of the scrutinized medium.

DOI: 10.1103/PhysRevE.86.046105 PACS number(s): 89.75.Fb, 89.75.Kd, 05.10.Gg, 02.50.−r

I. INTRODUCTION

Pattern formation is a rich and fascinating field of investigation that extends over distinct realms of applications, ideally embracing chemistry, biology, and physics. Complex and extremely beautiful patterns can in fact spontaneously emerge in spatially extended reaction–diffusion systems, as follows a linear instability mechanism, first described by Alan Turing in a seminal paper [1] published in 1952. Turing patterns are indeed widespread in nature: Examples include schemes of autocatalytic reactions with inhibition [2–4], the process of biological morphogenesis [5–9], and the dynamics of ecosystems [10–13]. The Turing instability paradigm classically relies on mean-field deterministic scenarios. As opposed to the usual continuum picture, the intimate discreteness of any individual-based stochastic models results in finite-size corrections to the approximated mean-field dynamics. Under specific conditions, microscopic disturbances are enhanced by a resonance mechanism and yield organized spatiotemporal patterns [14–17]. More specifically, the measured concentration that reflects the distribution of the interacting entities (e.g., chemical species and biomolecules) can display spatially patched profiles, collective phenomena which testify on a surprising degree of macroscopic order, as mediated by the stochastic component of the dynamics. Stochastic Turing patterns [16], or quasi-Turing patterns [15], are found to occur in individual-based systems that cannot undergo Turing instability according to the deterministic reaction-diffusion picture. Interestingly, the region of parameters for which stochastic patterns are developed is usually larger than for conventional Turing patterns, a general observation that has been made quantitative for a selection of prototypical case studies.

Recently, Nakao and Mikhailov [18] studied the Turing patterns formation on large random networks, an important direction of investigation presumably relevant in e.g. the early stage of the morphogenesis process, since morphogens are known to diffuse on the network structure of inter–cellular connections. Othmer and Scriven [19] investigated the Turing instability in a network-organized system and developed the needed mathematical machineries. Their studies, however, were limited to regular lattice or small networks. By extending the analysis to a complex heterogeneous network Nakao and Mikhailov [18] opened up the perspective for novel applications of the Turing idea to the broad field of theoretical biology [20]. Applications can be foreseen in other disciplines also where network science proves crucial. One example is social studies, in which nodes and links are associated with humans and their mutual interactions, respectively. Also interesting is the case of epidemics spreading, which is influenced by the topological structure of the underlying mobility networks.

Starting from this setting, we propose here a generalization of the work in Ref. [18], beyond the deterministic scenario, by explicitly including the role of demographic, finite-size fluctuations. In doing so, and with reference to the specific case of a scale-free network, we will demonstrate in this paper that *stochastic Turing patterns* set in outside the region of parameters corresponding to spatial order, as predicted within the classical theory based on deterministic reaction-diffusion schemes. This constitutes in turn the main result of our work. The analysis, which combines numerical and analytical tools, can be adapted in principle to other complex network structures, beyond the scale-free topology selected here for demonstrative purposes.

More concretely, we shall consider a stochastic version of the celebrated Brusselator model [2], which will be placed on top of a scale-free network of Ω nodes. The proposed microscopic formulation will make it possible to eventually reframe the mechanism of multispecies diffusion under crowded conditions, as discussed in Ref. [21], in a context relevant for network science. This is a side result of our analysis, which could prove interesting, however, for those applications that aim at tracking the physical transport, or flow of information, on densely populated networks.

II. THE STOCHASTIC MODEL ON A SCALE-FREE NETWORK

In the stochastic version of the Brusselator model, the individual entities X_i and Y_i are assigned to the generic node i and therein react according to the following chemical

reactions [16]:

$$\begin{aligned} A + E_i &\xrightarrow{a} A + X_i, \\ X_i + B &\xrightarrow{b} Y_i + B, \\ 2X_i + Y_i &\xrightarrow{c} 3X_i, \\ X_i &\xrightarrow{d} E_i. \end{aligned} \tag{1}$$

The symbol E_i stands for an empty case and formally amounts to imposing a finite carrying capacity in each node of the network. In other words, we assume that each node can host a maximum number N of molecules (or agents), including the vacancies.[1] Let us denote by n_i and m_i the total number of elements belonging to species X and Y, respectively, in node i. Hence the corresponding number of vacancies totals in $N - n_i - m_i$. The parameters a, b, c, and d in Eqs. (1) are the reaction rates, while the species A and B are enzymatic activators whose concentrations are supposed to remain constant during the dynamics and insensitive to the specific node. In practice, A and B display a homogeneous distribution on the network. In addition to the above activator-inhibitor rules, we assume that the molecules can migrate between neighboring nodes as dictated by the following reactions:

$$\begin{aligned} X_i + E_j &\xrightarrow{\mu} E_i + X_j, \\ Y_i + E_j &\xrightarrow{\delta} E_i + Y_j, \end{aligned} \tag{2}$$

where μ and δ are the diffusion coefficients characteristic of the two species and the subscript j denotes the generic node connected to i via the network structure. Similar equations govern the diffusion from node j towards node i. The migration from node i towards node j, and vice versa, can occur only if space allows. When no vacancies are available at the destination site, the diffusion is effectively, and self-consistently, impeded.[2] To complete the notation we introduce the Ω-dimensional vectors $\mathbf{n} = (n_1, \ldots, n_i, \ldots, n_\Omega)$ and $\mathbf{m} = (m_1, \ldots, m_i, \ldots, m_\Omega)$ that unequivocally identify the state of the system. Under the Markov hypothesis, the probability $P(\mathbf{n},\mathbf{m},t)$ of seeing the system at time t in state $(\mathbf{n},\mathbf{m})$ obeys the master equation

$$\begin{aligned} &\frac{\partial}{\partial t} P(\mathbf{n},\mathbf{m},t) \\ &= \sum_{i=1}^{\Omega} \Big(\big(\epsilon_{n_i}^- - 1\big) T(n_i + 1, m_i | n_i, m_i) \\ &\quad + \big(\epsilon_{n_i}^+ - 1\big) T(n_i - 1, m_i | n_i, m_i) \\ &\quad + \big(\epsilon_{n_i}^- \epsilon_{m_i}^+ - 1\big) T(n_i + 1, m_i - 1 | n_i, m_i) \\ &\quad + \big(\epsilon_{n_i}^+ \epsilon_{m_i}^- - 1\big) T(n_i - 1, m_i + 1 | n_i, m_i) \\ &\quad + \sum_{j=1}^{\Omega} W_{i,j} \big[\big(\epsilon_{n_i}^+ \epsilon_{n_j}^- - 1\big) T(n_i - 1, n_j + 1 | n_i, n_j) \\ &\quad + \big(\epsilon_{n_j}^+ \epsilon_{n_i}^- - 1\big) T(n_j - 1, n_i + 1 | n_i, n_j) \\ &\quad + \big(\epsilon_{m_i}^+ \epsilon_{m_j}^- - 1\big) T(m_i - 1, m_j + 1 | m_i, m_j) \\ &\quad + \big(\epsilon_{m_j}^+ \epsilon_{m_i}^- - 1\big) T(m_j - 1, m_i + 1 | m_i, m_j) \big] \Big) \\ &\quad \times P(\mathbf{n},\mathbf{m},t), \end{aligned} \tag{3}$$

where use has been made of the step operators $\epsilon_{n_i}^{\pm} f(\ldots, n_i, \ldots, \mathbf{m}) = f(\ldots, n_i \pm 1, \ldots, \mathbf{m})$ and $\epsilon_{m_i}^{\pm} f(\mathbf{n}, \ldots, m_i, \ldots) = f(\mathbf{n}, \ldots, m_i \pm 1, \ldots)$, with $f(\cdot,\cdot)$ being any generic function of the state variables. The $\Omega \times \Omega$ integers W_{ij} represent the entries of the symmetric adjacency matrix $\mathbf{W}$, which characterizes the topology of the network; W_{ij} is equal to 1 if nodes i and j are connected and 0 otherwise. The transition rates $T(\mathbf{n}',\mathbf{m}'|\mathbf{n},\mathbf{m})$ link the initial state $(\mathbf{n},\mathbf{m})$ to another state $(\mathbf{n}',\mathbf{m}')$, compatible with the former, and are given by[3]

$$\begin{aligned} T(n_i + 1, m_i | n_i, m_i) &= \frac{a}{\Omega} \frac{N - n_i - m_i}{N}, \\ T(n_i - 1, m_i | n_i, m_i) &= \frac{d}{\Omega} \frac{n_i}{N}, \\ T(n_i + 1, m_i - 1 | n_i, m_i) &= \frac{c}{\Omega} \frac{n_i^2 m_i}{N^3}, \\ T(n_i - 1, m_i + 1 | n_i, m_i) &= \frac{b}{\Omega} \frac{n_i}{N}, \\ T(n_i - 1, n_j + 1 | n_i, n_j) &= \frac{\mu}{\Omega} \frac{n_i}{N} \frac{N - n_j - m_j}{N} \left(\frac{1}{k_i} + \frac{1}{k_j} \right), \\ T(m_i - 1, m_j + 1 | m_i, m_j) &= \frac{\delta}{\Omega} \frac{m_i}{N} \frac{N - n_j - m_j}{N} \left(\frac{1}{k_i} + \frac{1}{k_j} \right), \end{aligned}$$

where $k_i = \sum_{j=1}^{\Omega} W_{ij}$ is the degree of the ith node. The factor $1/k_i + 1/k_j$ takes into account the order of selection of species in chemical reactions (2). To explain the origin of such term let us consider the first of Eqs. (2). Imagine that X_i is selected at first. Then the reaction can involve any of the vacancies E_j, with node j connected to node i, which could eventually represent a possible target for the migrating molecule. As all targets are equivalent, the transition rates need to be properly normalized. This is achieved by dividing the probability of the encounter for the connectivity k_i of node i. Similar considerations apply to the alternative scenario, when the empty case E_j on node j is picked up at first. In this case, one needs to introduce the normalizing scaling factor $1/k_j$.

The master equation (3) is exact although difficult to handle. To progress in the analysis it is customary to resort to approximated perturbation methods. In the weak noise approximation,

[1] By imposing a finite carrying capacity on each node we obtain a self-consistent formulation that holds under both diluted and crowded conditions. As we shall comment later, it also enables us to introduce an invariant quantity of the dynamics, the number of elements hosted in each node, which will prove central in the forthcoming analytical calculation. For a discussion of the role played by the finite carrying capacity we refer to Refs. [14,21–23].

[2] Under diluted conditions, the mutual interference that results from the competition for the microscopic spatial resources becomes negligible. The vacancies can hence be omitted in the above chemical equations. One obtains a different model, less general from our perspective, which can be inspected, however, with analogous techniques (see Ref. [23]), yielding to qualitatively similar conclusions.

[3] Notice that in the first and fourth transition rates, the constant (node-independent) concentrations relative to the enzymatic species A and B have been formally absorbed in the chemical rates a and b.

one can put forth the van Kampen ansatz [24,25], which, in this context, amounts to imposing $n_i/N = \phi_i + \xi_{1i}/\sqrt{N}$ and $m_i = \psi_i + \xi_{2i}/\sqrt{N}$, where ϕ_i and ψ_i are the mean-field concentrations associated with the interacting species X and Y, respectively, and ξ_{1i} and ξ_{2i} are stochastic fluctuations that originate from finite-size corrections, normalized by the scaling factor $1/\sqrt{N}$, as dictated by the central limit theorem [24]. For moderately large system sizes N, the $1/\sqrt{N}$ factor is small and paves the way to a straightforward perturbative calculation, generally referred to in the literature as the van Kampen system size expansion. At the leading order of the perturbative analysis, the mean-field equations for the deterministic variables are recovered and for the specific problem investigated here read

$$\begin{aligned}\frac{d}{d\tau}\phi_i &= f(\phi_i,\psi_i) \\ &\quad + 2\mu\left[\sum_{j=1}^{\Omega}\Delta_{ij}\phi_j + \phi_i\sum_{j=1}^{\Omega}\Delta_{ij}\psi_j - \psi_i\sum_{j=1}^{\Omega}\Delta_{ij}\phi_j\right], \\ \frac{d}{d\tau}\psi_i &= g(\phi_i,\psi_i) \\ &\quad + 2\delta\left[\sum_{j=1}^{\Omega}\Delta_{ij}\psi_j + \psi_i\sum_{j=1}^{\Omega}\Delta_{ij}\phi_j - \phi_i\sum_{j=1}^{\Omega}\Delta_{ij}\psi_j\right],\end{aligned} \tag{4}$$

where, generalizing the heuristic derivation of Ref. [18], we have introduced the discrete Laplacian $\Delta_{ij} = \tilde{W}_{ij} - \tilde{k}_i\delta_{ij}$ with $\tilde{k}_i = \sum_{j=1}^{\Omega}\tilde{W}_{ij}$ and $\tilde{W}_{ij} = (1/k_i + 1/k_j)W_{ij}$. The reaction terms are, respectively, $f = -(b+d)\phi_i + c\phi_i^2\psi_i + a(1-\phi_i-\psi_i)$ and $g = b\phi_i - c\phi_i^2\psi_i$ and τ is the rescaled time $t/N\Omega$. Cross diffusion terms appear in the deterministic equations obtained because of the finite carrying capacity, imposed at the level of the single node [21]. By relaxing such an assumption [23], conventional diffusion operators are recovered instead. Similarly, the finite carrying capacity assumption reflects in the reaction contribution $a(1-\phi_i-\psi_i)$, which replaces the usual constant term a in the standard Brusselator equations [16]. Although interesting *per se*, this modification does not play any substantial role in the forthcoming development: Equivalent conclusions can be drawn when working in the diluted setting, i.e., away from jamming or crowding conditions that inspire the physically sound request for a limited capacity to be explicitly accommodated on each individual node.

III. DETERMINISTIC TURING INSTABILITY

To look for mean-field Turing instability, one needs to introduce a small perturbation to the homogeneous equilibrium point $(\phi^*,\psi^*) = \{[a+\sqrt{a^2-4ab(a+d)/c}]/2/(a+d), b/c/\phi^*\}$ of the deterministic system (4) and carry out a linear stability analysis. In formulas, $(\phi_i,\psi_i) = (\phi^*+\delta\phi_i, \psi^*+\delta\psi_i)$. Following Ref. [18], and to exploit the linearity of the resulting equations for the perturbation amounts,[4] we find it convenient to expand $\delta\phi_i$ and $\delta\phi_i$ as

$$\delta\phi_i = \sum_{\alpha=1}^{\Omega} c_\alpha e^{\lambda_\alpha\tau}v_i^{(\alpha)}, \quad \delta\psi_i = \sum_{\alpha=1}^{\Omega} c_\alpha\beta_\alpha e^{\lambda_\alpha\tau}v_i^{(\alpha)}, \tag{5}$$

where $\mathbf{v}^{(\alpha)} = (v_1^{(\alpha)},\ldots,v_\Omega^{(\alpha)})$ stand for the eigenvectors of the Laplacian operator corresponding to the eigenvalue Λ_α.[5]

By inserting Eqs. (5) into the linearized differential equation for the perturbations $\delta\phi_i$ and $\delta\psi_i$, one obtains the usual characteristic equation for λ_α, which can be cast here in the form

$$\det\begin{pmatrix} f_\phi + \mu(1-\psi^*)\Lambda_\alpha - \lambda_\alpha & f_\psi + \mu\phi^*\Lambda_\alpha \\ g_\phi + \delta\psi^*\Lambda_\alpha & g_\psi + \delta(1-\phi^*)\Lambda_\alpha - \lambda_\alpha\end{pmatrix} = 0, \tag{6}$$

where $f_q = \partial f/\partial q$ and $g_q = \partial g/\partial q$ for $q = \phi,\psi$.

The Turing instability occurs and the perturbation thus gets amplified if $\lambda_\alpha(\Lambda_\alpha)$ is positive for some value of Λ_α. In this respect, and as already remarked in Ref. [18], Λ_α plays the role of $-k^2$ for continuous media, where k stands for the wave number of the plane wave mode. In Fig. 1(b) the dispersion relation is plotted for two distinct choices of the parameters (see the legend). Symbols refer to the discrete linear growth rates λ_α, as functions of the corresponding Laplacian eigenvalues Λ_α. The solid line represents the homologous dispersion relations, as obtained working within the continuous representation ($\Lambda_\alpha \to -k^2$). The top curve [Fig. 1(b), circles] signals the presence of an instability. A significant fraction of the discrete rates λ_α is in fact positive. Conversely, the other profile (diamonds) is obtained for a choice of the chemical parameters that yields linear stability. By tuning the parameters and evaluating the corresponding dispersion relation, one can eventually single out in a reference parameter space the region deputed to the instability. This is done in Fig. 1(a) working in the (b,c) plane: The region of Turing instability, as predicted by the deterministic analysis, is filled with a uniform color (yellow). The (blue) diamond falls outside the region of Turing order and points to the parameters employed in depicting the stable dispersion curve in Fig. 1(b). Similarly, the (magenta) circle refers to the unstable profile. In this latter case, performing a direct integration of the mean-field equations (4), one observes the spontaneous differentiation in activator-rich and activator-poor groups, as discussed in Ref. [18]. A stochastic simulation can also be carried out using an *ad hoc* implementation of the Gillespie Monte Carlo scheme [27]. In Ref. [28] the two dynamics, deterministic vs stochastic, are compared. Finite-size fluctuations materialize

[4]It is straightforward to show that the perturbations obey $\delta\dot{\phi}_i = f_\phi\delta\phi_i + f_\psi\delta\psi_i + \mu[(1-\psi^*)\sum_{j=1}\Delta_{ij}\delta\phi_j + \phi^*\sum_{j=1}\Delta_{ij}\delta\psi_j]$ and $\delta\dot{\psi}_i = g_\phi\delta\phi_i + g_\psi\delta\psi_i + \delta[(1-\phi^*)\sum_{j=1}\Delta_{ij}\delta\psi_j + \psi^*\sum_{j=1}\Delta_{ij}\delta\phi_j]$ under the linear approximation.

[5]The Laplacian operator Δ_{ij} is defined by the real and symmetric matrix $\Delta_{ij} = \tilde{W}_{ij} - \tilde{k}_i\delta_{ij}$, where k_i is the degree of node i. Eigenvectors $\mathbf{v}^{(\alpha)}$ and eigenvalues Λ_α are calculated by solving the eigenvalue problem $\sum_{j=1}^{\Omega}\Delta_{ij}v_i(\alpha) = \Lambda_\alpha v_i^{(\alpha)}$, with $\alpha = 1,\ldots,\Omega$. The computed eigenvalues are real and nonpositive. The eigenvectors are orthonormalized so as to match the condition $\sum_i v_i^{(\alpha)}v_i^{(\beta)} = \delta_{\alpha,\beta}$.

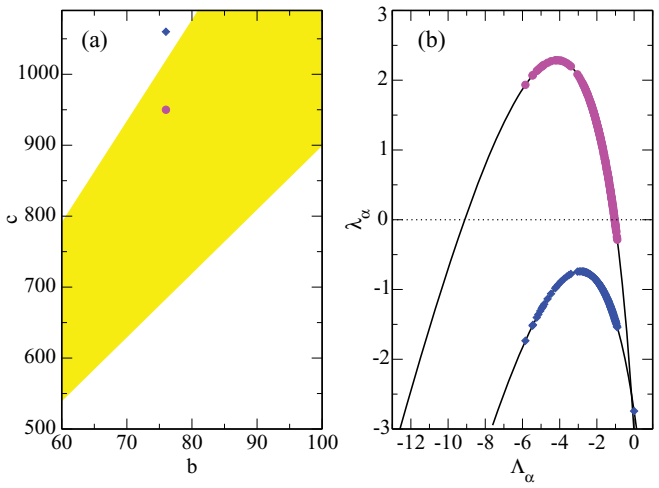

FIG. 1. (Color online) (a) The shaded (yellow) region delineates the Turing instability domain in the (b,c) plane for the Brusselator model with $a = d = 1$, $\mu = 1$, and $\delta = 15$. The (magenta) point belongs to the Turing instability region and corresponds to $b = 76$ and $c = 950$. The (blue) diamond falls outside the region of Turing order and is positioned at (76,1060). (b) Dispersion relation (6) plotted as a function of both the discrete eigenvalues of the network Laplacian (symbols) and their real analogs $-k^2$ (solid line). Circles (magenta) refer to $(b,c) = (76,950)$, while diamonds (blue) refer to $(b,c) = (76,1060)$. In the analysis we assumed a scale-free network made of $\Omega = 200$ nodes and mean degree $\langle k \rangle = 20$. The network has been generated according to the Barabási-Albert algorithm [26].

in a modest perturbation (proportional to $1/\sqrt{N}$) of the idealized mean-field dynamics.

IV. ANALYSIS OF FLUCTUATIONS: STOCHASTIC TURING PATTERNS

Substantially different is the scenario that is eventually recovered when comparing the simulations outside the region deputed to Turing instability. Setting the parameters to the values ($b = 76$ and $c = 1060$) that correspond to the (blue) diamond of Fig. 1(a), the deterministic simulations always converge to the homogeneous fixed point, the concentrations of the species therefore being identical on each node of the network. At variance, a fragmentation into distinct groups is clearly observed in the stochastic simulations. The late time evolution of the stochastic system, as compared to the corresponding (trivial) deterministic solution, is displayed in Fig. 2. The effect of the stochastically driven polarization can be further realized when inspecting the movies in Ref. [28], which enables one to appreciate the full time evolution of the discrete dynamics. As for the case of continuous media, the endogenous stochastic noise is amplified and drives the formation of spatially extended self-organized patterns outside the region of classical Turing order.[6] Following Ref. [16], we

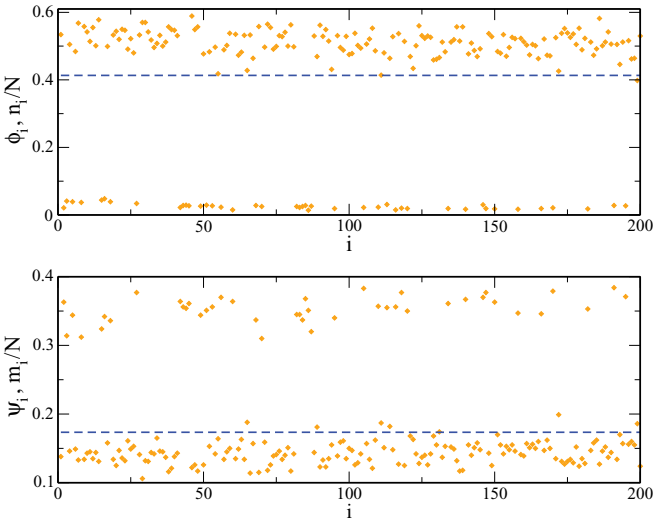

FIG. 2. (Color online) Simulations of the stochastic chemical model (1) and (2) outside the region of Turing order, $a = d = 1$, $b = 76$, $c = 1060$, $\mu = 1$, and $\delta = 15$. Here $N = 1000$. The late time concentrations per node n_i/N (m_i/N) are plotted in the top (bottom) panel as a function of the node index i. Nodes are sorted according to their degree, from large to small connectivities k_i. The (orange) diamonds are obtained from one realization of the stochastic Gillespie algorithm [27]. The network is generated as described in the caption of Fig. 1. The stochastic dynamics yields the emergence of two distinct activator-rich and activator-poor groups, while the deterministic dynamics is attracted towards the stable (and trivial) homogeneous fixed point [dashed (blue) horizontal line].

call these self-organized asymptotically stable configurations stochastic Turing patterns on a network.

To gain analytic insight into the above mechanism, one can return to the van Kampen perturbative analysis and consider the next to leading approximation. One obtains a system of Langevin equations [14,16] for the fluctuations ξ_{si} ($s = 1,2$):

$$\frac{d\xi_{si}}{d\tau} = \sum_{r,j} \mathcal{M}_{sr,ij}\xi_{rj} + \eta_{si}(\tau), \tag{7}$$

where η_{si} is a Gaussian noise with zero mean and the correlator given by $\langle \eta_{si}(\tau)\eta_{rj}(\tau')\rangle = \mathcal{B}_{sr,ij}\delta_{\tau\tau'}$. The explicit form of the matrices $\mathcal{M}$ and $\mathcal{B}$ is given in Ref. [28]. Define then the following transformation:

$$\tilde{\xi}_\alpha = \sum_{i,\tau} \xi_i e^{-j\omega\tau} v_i^{(\alpha)}, \tag{8}$$

with j denoting here the imaginary unit. The above operation is inspired by the Fourier transform: Instead of expanding on the basis of plane waves, it is natural here to project the fluctuations along the Ω-independent directions represented by the eigenvectors $\mathbf{v}^{(\alpha)}$ of the discrete network Laplacian. One can hence define a power spectrum of fluctuations of species $s = 1,2$, $P_s(\omega,\Lambda_\alpha) = \langle|\tilde{\xi}_s|^2\rangle$, in complete analogy to what is customarily done in conventional Fourier analysis. In practical

[6]The number of nodes in the fragmented state that respectively display high and low concentrations is approximately constant in time. This observation follows a dynamical balance: The nodes are continuously, although rarely, switching from high to low concentrations, the transitions being more frequent when the system size N gets reduced.

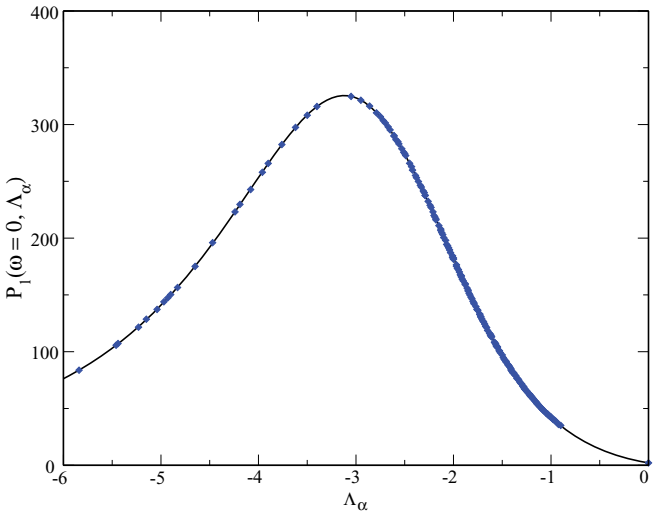

FIG. 3. (Color online) Power spectrum of fluctuations for species X as a function of Λ_α, $\omega = 0$ (symbols). The solid line is the power spectrum calculated for a continuum medium, i.e., when Λ_α is replaced by $-k^2$, where k denotes the wave number of the plane-wave mode. The curve refers to $a = d = 1$, $b = 76$, $c = 1060$, $\mu = 1$, and $\delta = 15$, a choice of parameters that corresponds to operating outside the region of Turing instability [diamond in Fig. 1(a)]. The network is constructed as specified in the caption of Fig. 1.

terms, the generalized power spectrum $P_s(\omega, \Lambda_\alpha)$ quantifies the portion of the signal power that is associated with a given time ω or spatial frequency Λ_α range. Some details of the calculations are given in Ref. [28].

In Fig. 3 the analytical power spectrum of species X is plotted in the plane $\omega = 0$, as a function of Λ_α, for a parameter selection that corresponds to the diamond in Fig. 1, i.e., outside the region of deterministic Turing instability. Symbols are obtained by sampling the power spectrum over the discrete Laplacian eigenvalues Λ_α. The solid line stands for the power spectrum calculated in the continuous limit when the discrete Λ_α is replaced with its real counterpart $-k^2$ (see Ref. [28] for a discussion related to this point). A clear peak is displayed,[7] a finding that explains in turn the outcome of the stochastic-based simulations reported in Fig. 2, formally proving that stochastic Turing patterns do exist on a network topology.

[7]Similar conclusions hold for the power spectrum of species Y.

V. CONCLUSIONS

In conclusion, we have considered in this paper the stochastic dynamics of the Brusselator model on a scale-free network. The model, representative of a broad class of systems that display Turing order in the mean-field limit, has been investigated both analytically and numerically. In particular, we provide evidence of the intrinsic ability of the system to develop spatially heterogeneous configurations, outside the region of parameters classically deputed to Turing (deterministic) order. These self-organized patterns, reminiscent of the Turing instability, result from the spontaneous amplification of the demographic noise, stemming from the intimate discreteness of the scrutinized medium. Our analysis therefore extends the concept of stochastic Turing order to the vast domain of network science, a discipline of paramount importance and cross-disciplinary interests. Further investigations can be planned working along these lines (and so explore the surprising degree of macroscopic order that can eventually originate from the noisy microscopic dynamics) for stochastic based systems defined on a network topology. As an example, stochastic traveling waves can be imagined to occur as a natural extension of Ref. [23]. Incidentally, we also emphasize that the finite carrying capacity mechanism imposed here at the node level could be useful in modeling those phenomena where jamming on a network topology is expected to occur.

ACKNOWLEDGMENTS

Financial support from Ente Cassa di Risparmio di Firenze and the Program Prin2009 funded by Italian Ministero dell'Istruzione, dell'Università e della Ricerca (MIUR) is acknowledged. D.F. thanks Tommaso Biancalani for pointing out Ref. [18] and for stimulating discussions. F.D.P. thanks Alessio Cardillo for providing the code to generate the network.

[1] A. M. Turing, Philos. Trans. R. Soc. London Ser. B **237**, 37 (1952).
[2] I. Prigogine and R. Lefever, J. Chem. Phys. **48**, 1695 (1968).
[3] V. Castets, E. Dulos, J. Boissonade, and P. De Kepper, Phys. Rev. Lett. **64**, 2953 (1990).
[4] Q. Ouyang and H. L. Swinney, Nature (London) **352**, 610 (1991).
[5] H. Meinhardt and A. Gierer, BioEssays **22**, 753 (2000).
[6] M. P. Harris, S. Williamson, J. F. Fallon, H. Meinhardt, and R. O. Prum, Proc. Natl. Acad. Sci. USA **102**, 11734 (2005).
[7] P. K. Maini, R. E. Baker, and C. M. Chuong, Science **314**, 1397 (2006).
[8] S. A. Newman and R. Bhat, Birth Defects Res. C **81**, 305 (2007).
[9] T. Miura and K. Shiota, Dev. Dyn. **217**, 241 (2000).
[10] M. Mimura and J. D. Murray, J. Theor. Biol. **75**, 249 (1978).
[11] J. L. Maron and S. Harrison, Science **278**, 1619 (1997).
[12] M. Baurmann, T. Gross, and U. Feudel, J. Theor. Biol. **245**, 220 (2007).
[13] M. Rietkerk and J. van de Koppel, Trends Ecol. Evol. **23**, 169 (2008).
[14] A. J. McKane and T. J. Newman, Phys. Rev. Lett. **94**, 218102 (2005).
[15] T. Butler and N. Goldenfeld, Phys. Rev. E **80**, 030902(R) (2009).
[16] T. Biancalani, D. Fanelli, and F. Di Patti, Phys. Rev. E **81**, 046215 (2010).
[17] T. E. Woolley, R. E. Baker, E. A. Gaffney, and P. K. Maini, Phys. Rev. E **84**, 046216 (2011).

[18] H. Nakao and A. S. Mikhailov, Nat. Phys. **6**, 544 (2010).
[19] H. G. Othmer and L. E. Scriven, J. Theor. Biol. **43**, 83 (1974).
[20] R. Pastor-Satorras and A. Vespignani, Nat. Phys. **6**, 480 (2010).
[21] D. Fanelli and A. J. McKane, Phys. Rev. E **82**, 021113 (2010).
[22] C. A. Lugo and A. J. McKane, Phys. Rev. E **78**, 051911 (2008).
[23] T. Biancalani, T. Galla, and A. J. McKane, Phys. Rev. E **84**, 026201 (2011).
[24] N. G. van Kampen, *Stochastic Processes in Physics and Chemistry* (North-Holland, Amsterdam, 1992).
[25] C. W. Gardiner, *Handbook of Stochastic Methods*, 2nd ed. (Springer, Berlin, 1985).
[26] A. Barabási and R. Albert, Science **286**, 509 (1999).
[27] D. T. Gillespie, J. Comput. Phys. **22**, 403 (1976).
[28] See Supplemental Material at http://link.aps.org/supplemental/10.1103/PhysRevE.86.046105 for movies of the deterministic and stochastic dynamics and for some details about the analytical calculations.